Sixth International Symposium on Turbulence and Shear Flow Phenomena
Seoul, Korea, 22-24 June 2009

MODELLING CONCENTRATION FLUCTUATIONS FROM A LOCALIZED SOURCE IN COMPLEX URBAN TURBULENT FLOWS

Bing-Chen Wang
Dept. of Mechanical & Manufacturing Engineering, Univ. of Manitoba
Winnipeg, MB, R3T 5V6, Canada
E-mail: bc_wang@umanitoba.ca

Eugene Yee
Defence Research & Development Canada — Suffield
P.O. Box 4000, Medicine Hat, Alberta, T1A 8K6, Canada
E-mail: bingchen.wang@drdc-rddc.gc.ca, eugene.yee@drdc-rddc.gc.ca

Fue-Sang Lien
Dept. of Mechanical Engineering, Univ. of Waterloo
Waterloo, Ontario, N2L 3G1, Canada
E-mail: fslien@mecheng1.uwaterloo.ca

ABSTRACT

Turbulent dispersion of a passive scalar released from a continuous ground-level point-source in an idealized urban environment is studied using both the numerical and experimental approaches. The numerical simulation of the turbulent flow and dispersion fields is based on the Reynolds-averaged Navier-Stokes methods which uses nonlinear turbulent stress and scalar-flux models for the closure of momentum and scalar transport equations, respectively. The novel inner-scale based concentration variance dissipation model of Yee *et al.* (2009) is tested against two new sets of high-quality water-channel measurement data obtained using 1-D laser induced fluorescence (for concentration) and 2-D laser Doppler anemometer (for velocity).

INTRODUCTION

As the World's urban population grows, it is becoming increasingly important to assess effectively the hazards caused by potentially harmful materials released into the urban environment. Should such a release of a contaminant occur, it is important to be able to predict the dispersion of a hazardous contaminant within the urban canopy where human habitation is concentrated. Over the past decade, a considerable effort has been expended from the experimental, theoretical and numerical points of view to understand the flow and dispersion in the urban environment over a wide range of scales, from the very large at the regional and city scales to the quite small at the neighborhood and street (or building) scales.

Recently, a number of important field trials have been conducted to investigate urban flow and pollutant dispersion. Large-scale urban field studies in the United States have included the Mock Urban Setting Trial (MUST) conducted at U.S. Army Dugway Proving Ground in northwestern Utah in September 2001 (Yee and Biltoft, 2004), the Joint Urban 2003 Experiment conducted in Oklahoma City (Flaherty *et al.*, 2007), and the Urban Dispersion Program (UDP) conducted in New York City over the period from 2004 to 2007 (Allwine *et al.*, 2007). Important urban field studies have been conducted in Europe such as the Dispersion of Air Pollution and its Penetration into the Local Environment (DAPPLE) which investigated the characteristics of flow in a street canyon intersection in London, UK (Arnold *et al.*, 2004). Owing to the urgent need for high-quality data sets for the validation of numerical models for the prediction of passive scalar dispersion within an urban environment, a number of experimental studies that measure urban flow and dispersion in idealized building arrays have recently been conducted in wind tunnels (MacDonald *et al.*, 1998; Gailis and Hill, 2006; Yee *et al.*, 2006; Pascheke *et al.*, 2008) and water channels (Yee *et al.*, 2006).

The development of numerical models for the concentration variance (second-order moment of concentration) for urban plumes have been undertaken recently, including the work of Andronopoulos *et al.* (2002), Hsieh *et al.* (2007), Milliez and Carissimo (2008), Wang *et al.* (2009) and Yee *et al.* (2009). In the model of Wang *et al.* (2009), the dissipation length scale for concentration variance is determined by the characteristic motions of eddies smaller than the local plume scale in the initial meandering stage of plume development, and is limited by the integral length scale of turbulence when the local plume scale becomes larger than the energy containing eddies of the flow in the turbulent diffusive stage of plume development. In comparison with the model of Wang *et al.* (2009), the recent model of Yee *et al.* (2009) improves the formulation for the concentration variance dissipation rate by relating it to the inner time scale associated with relative dispersion. Thus far, this new model of Yee *et al.* (2009) has only been validated against one set of experimental data on a dispersing plume resulting from a continuous release of a passive tracer within a regular cubic obstacle array.

As a further advancement of our previous experimental and numerical studies of the concentration variance in the context of a complex urban-like environment, we report a new set of high-quality water-channel data for turbulent dispersion of a passive scalar released from a localized source in an aligned array of rectangular obstacles. Also, we apply a Reynolds-averaged Navier-Stokes (RANS) method to

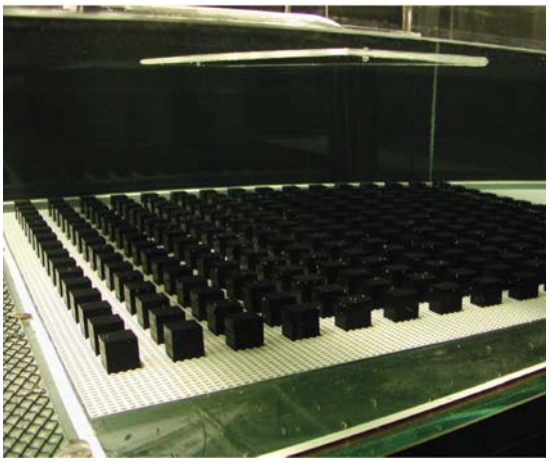

Fig. 1: Regular obstacle array in water channel (array-1H).

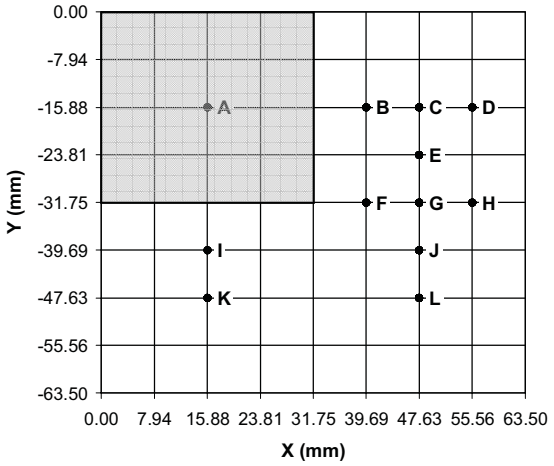

Fig. 2: Velocity measurement (or, sampling) locations in a cell ($2H \times 2H$, with $H = 31.75$ mm).

numerically simulate the physical processes of turbulent dispersion, and further validate the new model proposed by Yee *et al.* (2009) using the experimental data reported here.

EXPERIMENTAL MEASUREMENTS

Water channel simulations of flow and dispersion in different types of arrays were conducted at Coanda R&D Corporation (Burnaby, BC, Canada). A detailed description of the experiment can be found in the laboratory report of Hilderman and Chong (2007). The water channel used in the experiments is specially designed for studying flow and dispersion in idealized arrays of building-like obstacles. The test section of the water channel is 10 m × 1.5 m × 0.9 m [in the streamwise, spanwise and vertical directions (denoted by x, y and z), respectively]. Two different aligned arrays of rectangular obstacles with square cross-section of side length $H = 31.75$ mm and with heights of $1H$ and $2H$ are investigated. Henceforth, these two arrays will be referred to as "array-1H" (array of cubes) and "array-2H" (array of parallelepipeds). Fig. 1 shows one of the tested arrays (i.e., array-1H) in the water channel. Both tested arrays consist of 16×16 obstacles. The Reynolds number of the flow was approximately $Re_H = 12,005$ (based on H and the free stream velocity $U_b = 0.38$ m s^{-1}).

The velocity field was measured using a 4-beam 2-component TSI fibre-optic laser doppler anemometer (LDA) powered by an argon-ion laser. Titanium dioxide was used as seed particles. The LDA data were collected over a sampling time of 500 s at each position. The data rate for the LDA measurements depended upon the flow velocity, particle seeding density, and optical properties of the lenses, but was typically 50-500 Hz. Detailed measurements were taken at 12 locations in two cells near the centerline of the array. Here, a "cell" represents the basic repeating unit used to construct the obstacle array. A cell of the array occupies an area of $2H \times 2H$ in the x-y plane with the obstacle occupying the upper-left quadrant (shown shaded in Fig. 2) of the cell. Furthermore, Fig. 2 shows the locations for the velocity measurements in each unit cell, and Fig. 3 exhibits the coordinate system used in the problem definition. Measurements of the vertical profiles of velocity were made in the first (cell 1) and sixth (cell 6) cells in the downstream direction along the eighth column in the array of cubes (i.e., near the centerline of the array).

A 1-D laser induced fluorescence (LIF) linescan system

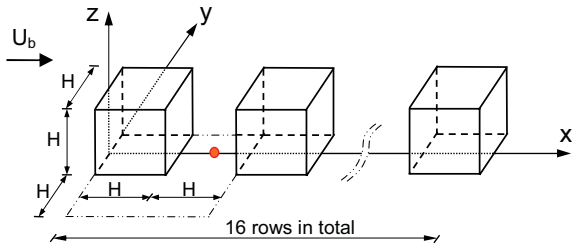

(a) Array-1H

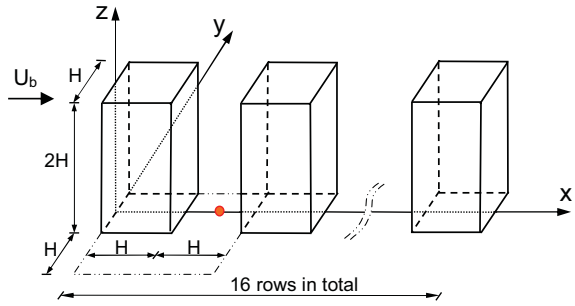

(b) Array-2H

Fig. 3: Geometry of the obstacle arrays in the water channel: central (or, 8th) column of the obstacles.

was used for measuring the instantaneous concentration field in the dispersing plume. Sodium fluorescein dye was continuously released from a point source at a rate of 12 ml min^{-1}, and illuminated using a laser beam powered by an argon-ion laser. The dye source was released from a small vertical stainless steel tube (with an inner diameter $d_0 = 2.8$ mm). A Dalsa monochrome digital linescan CCD camera (1024 × 1 pixels), 12-bit (4,096 gray levels) was used to measure the intensity of the dye fluorescence at a sampling rate of 300 Hz for a sampling time of 1,000 seconds at each measurement position. Although a number of ground-level and elevated point-source locations were used for both arrays in the experiments, we will focus here on only one particular ground-level point-source location in which the source is located in the midway between rows 1 and 2 along the central column of the obstacles (see Fig. 3 for the details).

NUMERICAL ALGORITHM AND MODELS

The velocity and concentration fields are described by the conservation laws for mass, momentum and concentration

for a neutrally-stratified incompressible flow, expressed in the usual ensemble-averaged form. In addition to these conservation laws, the transport equations for turbulence kinetic energy (TKE) k, the rate of dissipation ϵ of TKE and concentration variance $\overline{c'^2}$ are also used. These governing equations assume the following form in a Cartesian coordinate system:

$$\frac{\partial \bar{u}_i}{\partial x_i} = 0, \tag{1}$$

$$\frac{\partial \bar{u}_i}{\partial t} + \frac{\partial (\bar{u}_i \bar{u}_j)}{\partial x_j} = -\frac{\partial \bar{p}}{\partial x_i} + \frac{\partial}{\partial x_j}\left(\nu \frac{\partial \bar{u}_i}{\partial x_j}\right) - \frac{\partial \overline{u'_i u'_j}}{\partial x_j}, \tag{2}$$

$$\frac{\partial k}{\partial t} + \frac{\partial (\bar{u}_j k)}{\partial x_j} = \frac{\partial}{\partial x_j}\left[\left(\nu + \frac{\nu_t}{\sigma_k}\right)\frac{\partial k}{\partial x_j}\right] + P_k - \epsilon, \tag{3}$$

$$\frac{\partial \epsilon}{\partial t} + \frac{\partial (\bar{u}_j \epsilon)}{\partial x_j} = \frac{\partial}{\partial x_j}\left[\left(\nu + \frac{\nu_t}{\sigma_\epsilon}\right)\frac{\partial \epsilon}{\partial x_j}\right] + \frac{\epsilon}{k}(C_{\epsilon_1} P_k - C_{\epsilon_2}\epsilon), \tag{4}$$

$$\frac{\partial \bar{c}}{\partial t} + \frac{\partial (\bar{u}_j \bar{c})}{\partial x_j} = \frac{\partial}{\partial x_j}\left(D \frac{\partial \bar{c}}{\partial x_j}\right) - \frac{\partial \overline{u'_j c'}}{\partial x_j} + S, \tag{5}$$

$$\frac{\partial \overline{c'^2}}{\partial t} + \frac{\partial (\bar{u}_j \overline{c'^2})}{\partial x_j} = \frac{\partial}{\partial x_j}\left(D \frac{\partial \overline{c'^2}}{\partial x_j} - \overline{u'_j c'^2}\right) - 2\overline{u'_j c'}\frac{\partial \bar{c}}{\partial x_j} - \epsilon_c. \tag{6}$$

Here, $\bar{u}_i$ is the mean velocity in the i-th direction, $\bar{p}$ is the kinematic pressure, $\bar{c}$ is the mean concentration, S is the source density function of the tracer, D is the molecular diffusivity of the scalar, ν is the kinematic viscosity of the fluid, and $\nu_t \stackrel{\text{def}}{=} C_\mu k^2/\epsilon$ is the kinematic eddy viscosity. Eqs. (1)–(4) represent the standard k–ϵ model for the prediction of a turbulent velocity field. The closure constants are given as follows: $C_\mu = 0.09$, $\sigma_k = 1.0$, $C_{\epsilon 1} = 1.44$ and $C_{\epsilon 2} = 1.92$.

The numerical simulations were performed using two in-house computer codes: namely, urbanSTREAM for prediction of the turbulent velocity field and urbanEU for the prediction of the turbulent dispersion of the scalar field. Both codes apply a general curvilinear, second-order accurate, fully conservative and implicit finite-volume method for the discretization of the transport equations for momentum and scalar quantities. The flow solver in urbanSTREAM is based on numerical algorithms described by Lien and Leschziner (1994). The SIMPLE algorithm was used for the pressure correction. Checkerboard oscillations in the pressure field arising from a state of pressure-velocity decoupling on a collocated grid were removed using a nonlinear momentum interpolation scheme. Detailed descriptions of the algorithms underlying urbanSTREAM and urbanEU can be found in Yee *et al.* (2007).

The computational domain consists of 16 rows and 9 columns of cubes, with a spatial extent of $61H \times 18H \times 11H$ in the streamwise, spanwise, and wall-normal directions, respectively. A non-uniform coarse grid of $245 \times 149 \times 48$ control volumes was used for the discretization of the computational domain. Fig. 3 displays the geometry of the two arrays, whereas Fig. 4 shows the grid used in our simulation of array-1H. As shown in Fig. 4, the grid lines have been refined close to the source location and near every solid surface. At each solid surface, wall boundary conditions were applied for the velocity field (i.e., for the mean velocity and turbulence quantities k and ϵ), and zero-flux boundary conditions were used for the concentration and concentration variance fields.

At the inlet, Dirichlet boundary conditions were used for both the mean velocity and concentration fields. The inlet flow conditions for the mean velocity and TKE were obtained from the experimental measurements. The values of concentration and concentration variance at the inlet were set to zero. An upstream fetch of $15H$ (distance between the inlet plane and the windward face of the first row of obstacles) was used in our simulations. For all flow variables, zero-flux boundary conditions were applied at the upper free surface of the computational domain, Neumann boundary conditions were used at the outlet plane, and periodic boundary conditions were applied in the spanwise direction.

Turbulent Stress and Scalar-Flux Models. In order to close the governing equations, the kinematic Reynolds stresses (i.e., $\overline{u'_i u'_j}$) and turbulent fluxes of concentration and concentration variance (i.e., $\overline{u'_j c'}$ and $\overline{u'_j c'^2}$, respectively) need to be modelled. We use an explicit algebraic nonlinear Reynolds stress model [(viz., the quadratic model of Speziale (1987)] to close the mean momentum equation:

$$\begin{aligned}\overline{u'_i u'_j} = \frac{2}{3}k\delta_{ij} - \nu_t\left(\frac{\partial \bar{u}_i}{\partial x_j} + \frac{\partial \bar{u}_j}{\partial x_i}\right) + \frac{k^3}{\varepsilon^2}\Bigg[C_{\tau 1}\left(\frac{\partial \bar{u}_i}{\partial x_k}\frac{\partial \bar{u}_j}{\partial x_k}\right)^* \\ + C_{\tau 2}\left(\frac{\partial \bar{u}_i}{\partial x_k}\frac{\partial \bar{u}_k}{\partial x_j} + \frac{\partial \bar{u}_j}{\partial x_k}\frac{\partial \bar{u}_k}{\partial x_i}\right)^* + C_{\tau 3}\left(\frac{\partial \bar{u}_k}{\partial x_i}\frac{\partial \bar{u}_k}{\partial x_j}\right)^*\Bigg],\end{aligned} \tag{7}$$

where δ_{ij} is the Kronecker delta, and an asterisk indicates the deviatoric part of a tensor, i.e. $(\cdot)^*_{ij} \stackrel{\text{def}}{=} (\cdot)_{ij} - (\cdot)_{kk}\delta_{ij}/3$. The three model coefficients appearing in this equation are: $C_{\tau 1} = 0.041$, $C_{\tau 2} = 0.014$ and $C_{\tau 3} = -0.014$. For the turbulent scalar fluxes, we used the tensor diffusivity model of Yoshizawa (1985), viz.

$$\overline{u'_j c'} = -D_{jk}\frac{\partial \bar{c}}{\partial x_k} \quad \text{and} \quad \overline{u'_j c'^2} = -D_{jk}\frac{\partial \overline{c'^2}}{\partial x_k}, \tag{8}$$

where the tensor diffusivity D_{jk} is defined as

$$D_{jk} = C_{s1}\frac{k^2}{\varepsilon}\delta_{jk} + C_{s2}\frac{k^3}{\varepsilon^2}\left(\frac{\partial \bar{u}_j}{\partial x_k} + \frac{\partial \bar{u}_k}{\partial x_j}\right). \tag{9}$$

Here, $C_{s1} = 0.134$ and $C_{s2} = -0.032$ are two model coefficients.

Concentration Variance Dissipation Model. The critical term in the closure of Eq. (6) is the scalar dissipation: $\epsilon_c \stackrel{\text{def}}{=} 2D\frac{\partial c'}{\partial x_j}\frac{\partial c'}{\partial x_j}$. The modelling of ϵ_c determines effectively the rate at which internal concentration fluctuations in the dispersing plume are destroyed by the molecular diffusion. In this study, we further test the model recently proposed by Yee *et al.* (2009) against two sets of experimental data (i.e. the turbulent flow and dispersion data sets for array-1H and array-2H). The preliminary results for case array-1H have been discussed in Yee *et al.* (2009).

The model of Yee *et al.* (2009) is constructed based on the physical process illustrated in Fig. 5, which shows the spatial development of a plume from a compact (localized) source within the framework of a fluctuating plume model. Turbulent eddies on a wide range of scales exist in the atmosphere and act on the plume, resulting in a number of regimes in the spatial development of the plume. Turbulent eddies of size $l_e \gg \sigma_r$, where σ_r is the width of the instantaneous plume, results in the bulk meandering of the instantaneous plume (external fluctuations). Eddies with size $l_e \approx \sigma_r$ cause distortion of the instantaneous plume boundary as clean air packets are entrained into the body of the plume, resulting in the growth of σ_r. Hence, σ_r corresponds to an inner plume length scale of turbulent diffusion associated with internal fluctuations and so is connected with the process of relative dispersion. Therefore, the dissipation length scale Λ_d is intimately related to inner plume scale σ_r, rather than the outer (external) plume scale σ_a.

In view of this, the model of Yee *et al.* (2009) assumes

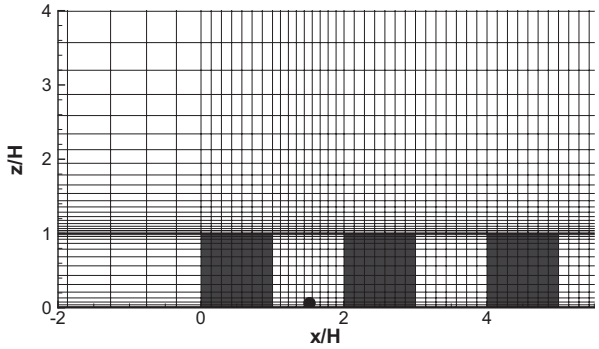

(a) x-z view

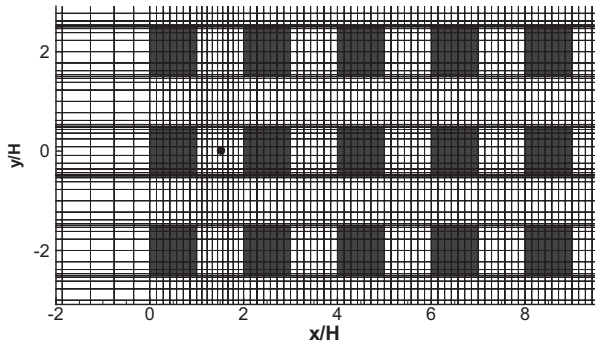

(b) x-y view

Fig. 4: A portion of the grid system (array-1H).

that:

$$\epsilon_c = c_1 \frac{\Delta v(\Lambda_d)}{\Lambda_d} \overline{c'^2}. \quad (10)$$

Here, $c_1 = 1.4$ is a closure constant and $\Delta v(\Lambda_d)$ is the characteristic velocity scale for turbulent eddies whose "size" is Λ_d. The dissipation time scale $t_d \propto \Lambda_d/\Delta v(\Lambda_d)$ corresponds to the eddy turn-over time for eddies that are comparable in size to the mean width of the instantaneous plume, as it is these eddies that are responsible for the in-plume concentration fluctuations and the concomitant scalar dissipation. Here, the characteristic velocity scale is modelled as

$$\Delta v(\Lambda_d) = k^{1/2} \min\left((\Lambda_d/\Lambda_I)^{1/3}, 1\right), \qquad \Lambda_d \geq \sigma_0, \quad (11)$$

where $\Lambda_I \stackrel{\text{def}}{=} k^{3/2}/\epsilon$ is the integral scale of turbulence and σ_0 is the initial source size. The dissipation length scale Λ_d for the concentration variance is determined using the following blending function:

$$\Lambda_d^2 = \frac{l_e^2}{1 + (l_e^2 - \sigma_0^2)/(\sigma_0^2 + c_2 D_t t)}, \quad (12)$$

where $c_2 = 2.7$ is a closure coefficient, t is the travel time, D_t is the turbulent eddy diffusivity, and l_e is the characteristic turbulent eddy size whose growth is determined using the Richardson-Obukhov 4/3-law for relative dispersion.

RESULTS AND ANALYSIS

Fig. 6 displays the isopleths of the mean concentration (non-dimensionalized using the source concentration c_s) in a horizontal x-y plane at one-half the canopy height for the array-1H case. The mean plume concentration profiles in the spanwise direction have a Gaussian distribution (approximately or better) provided that the downwind distance from the source is sufficiently large.

Figs. 7(a) and (b) compare the predicted mean velocity profiles with two sets of 2-D LDA measurements (i.e., the u-v and u-w configurations) at location C (see Fig. 2) in

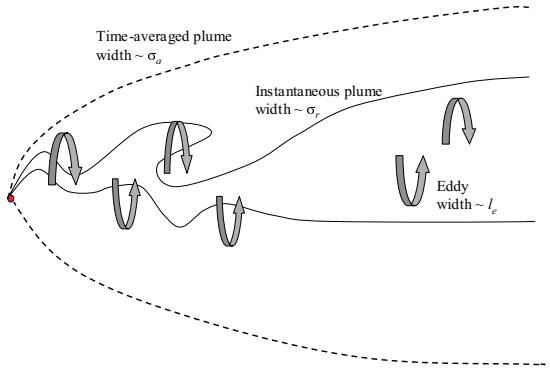

Fig. 5: A schematic of dispersion from a compact source within the framework of a fluctuating plume model.

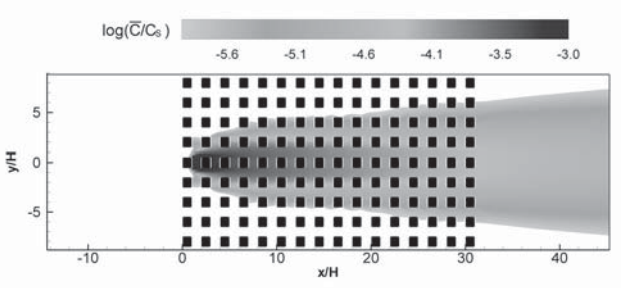

Fig. 6: Isopleths of the normalized mean concentration field in the horizontal x-y plane ($z/H = 0.5$, array-1H).

cells 1 and 6 near the centerline of array-1H. The agreement between the predicted and experimental results is excellent. From the figures, it is observed that the numerical simulations have successfully captured the very strong shear layer near the top of the obstacles (or at height $1H$). Furthermore, the magnitude of the reverse flow ($\bar{u}_1 < 0$) downstream of the leeward face of the obstacle (within the canopy for $z/H < 1$) is correctly reproduced by the simulation. Figs. 8(a) and (b) show the predicted TKE profiles in comparison with the experimental results in cells 1 and 6 near the centerline of array-1H. As seen in Fig. 8, for the standard k–ϵ approach, the level of TKE is generally underpredicted, especially in terms of the prediction of the maximum value of TKE. This observation is consistent with the results reported by Hsieh *et al.* (2007) and Wang *et al.* (2009) in their simulations of obstacle array flows.

Figs. 9 and 10 compare the predicted mean velocity and TKE profiles with the 2-D LDA measurements at location C in cells 1 and 6 near the centerline of array-2H. As in Figs. 7(a) and (b), we note that a very strong shear layer is present also in array-2H (cf. Figs. 9(a) and (b)), with a location at or near the top of the canopy (viz., at $z/H \approx 2$ for array-2H). Another observation is that the reverse flow pattern within the canopy for array-2H (cf. Fig. 9) is distinct from that for array-1H (cf. Fig. 7) due to the different heights of obstacles in two arrays. Figs. 11 and 12 show the mean velocity and TKE profiles at location L (the crossing of two canyons, see Fig. 2) in cells 1 and 6 for array-2H. In contrast to Fig. 9 (corresponding to location C lying midway in the recirculation zone between two obstacles), the strong shear layer in Fig. 11 is displaced downwards to the near ground level owing to the absence of obstacles at location L. Also, the reverse flow region disappears at location L, demonstrating the sensitivity of the flow dynamics to the physical location in a complex obstacle array. The reverse flow at location C in Fig. 9 is due to the recirculation of the flow behind an obstacle, which is absent at location L.

Figs. 13 and 14 compare predictions and measurements of

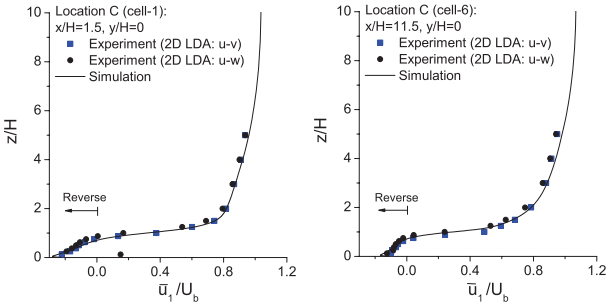

(a) Cell 1 (b) Cell 6

Fig. 7: Comparison of mean velocity at location C in cells 1 and 6 (array-1H).

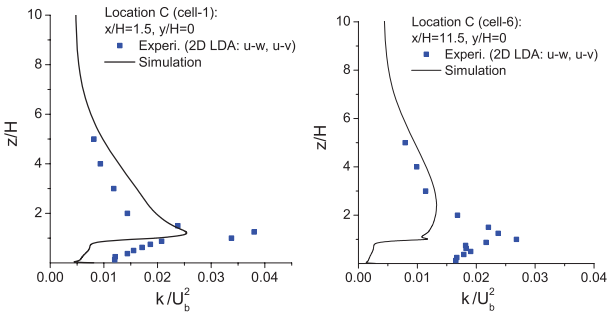

(a) Cell 1 (b) Cell 6

Fig. 8: Comparison of TKE at location C in cells 1 and 6 (array-1H).

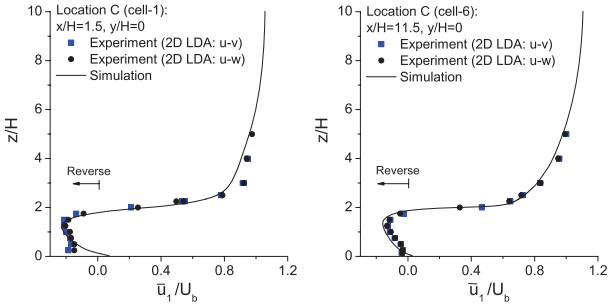

(a) Cell 1 (b) Cell 6

Fig. 9: Comparison of mean velocity at location C in cells 1 and 6 (array-2H).

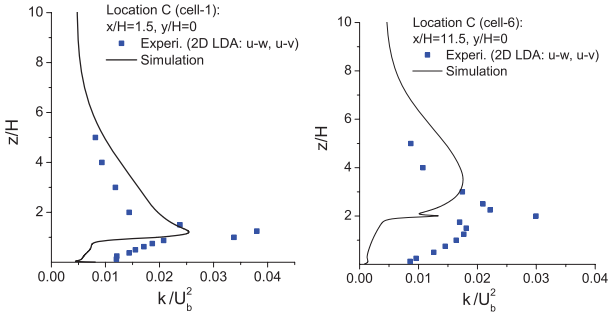

(a) Cell 1 (b) Cell 6

Fig. 10: Comparison of TKE at location C in cells 1 and 6 (array-2H).

the mean concentration $\bar{c}$ and standard deviation of concentration $(\overline{c'^2})^{1/2}$ [or root-mean-square (RMS) concentration], at half-canopy height ($z/H = 0.5$) at two fixed sampling locations downwind of the source (i.e., $x/H = 5.5$ and $x/H = 7.5$, respectively) in array-1H. It is seen from Figs. 13(a) and 14(a) that the shapes of the mean concentration profiles are correctly predicted by the model. In particular, the model correctly predicts the non-Gaussian distribution of the crosswind mean concentration profile, which is seen to exhibit a distinctly bimodal form due to the bifurcation of the plume as it sweeps around the sides of an obstacle. From both Figs. 13(b) and 14(b), it is seen that the numerical predictions of $(\overline{c'^2})^{1/2}$ are in good conformance with the measurements. Fig. 15(a) and 15(b) compare the measured and predicted vertical profiles of $\bar{c}$ and $(\overline{c'^2})^{1/2}$ at a fixed downstream location ($x/H = 3.5$) along the centerline ($y/H = 0$) of array-2H. By comparing Figs. 13, 14 and 15, it is observed that the agreement between the numerical and experimental results of $\bar{c}$ and $(\overline{c'^2})^{1/2}$ is better for the horizonal profiles than for the vertical profiles. This is because the vertical profiles of $\bar{c}$ and $(\overline{c'^2})^{1/2}$ are more sensitive to the precise lateral positioning in a plume than the horizontal profiles, which in turn makes the measurement of the vertical profiles based on the LIF more challenging in an experiment, especially in the near-wall region.

CONCLUSIONS

The dispersion of a passive tracer released from a continuous ground-level point-source in and above two arrays of rectangular obstacles has been studied using both the experimental and numerical methods. The numerical simulation is based on a RANS model which uses an algebraic nonlinear stress closure model for the Reynolds stress, a tensor diffusivity closure model for the scalar-fluxes, and a novel model for the concentration variance dissipation rate.

From a theoretical point of view, the concentration variance dissipation rate model of Yee *et al.* (2009) is very attractive since it embodies the basic physics of in-plume concentration fluctuations related to relative dispersion that are responsible for turbulent mixing and dissipation. The RANS prediction of the velocity, TKE, mean concentration and concentration variance for both array-1H and array-2H are generally satisfactory. The preliminary result of the array-1H case has been discussed in Yee *et al.* (2009). Here, we further confirm the good performance of this new model by testing it against a new set of high-quality water-channel measurement data (i.e., case array-2H) on turbulent flow and dispersion in an idealized urban environment.

REFERENCE

Andronopoulos S., Grigoriadis D., Robins A., Venetsanos A., Rafailidis S., Bartzis J. G. (2002), Three-dimensional modeling of concentration fluctuations in complicated geometry. *Environ. Fluid Mech.*, **1**:415–440.

Allwine, K. J., Clawson, K. L., Flaherty, J. E., Heiser, J. H., Hosker, R. P., Leach, M. J., and Stockham, L. W. (2007), Urban dispersion program: Urban measurements applied to emergency response. Seventh Symposium on the Urban Environment, American Meteorological Society, San Diego, California, 5 pp.

Arnold, S. J., ApSimon, H., Barlow, J., Belcher, S., Bell, M., Boddy, J. W., Britter, R., Cheng, H., Clark, R., Colvile, R. N., Dimitroulopoulou, S., Dobre, A., Greally, B., Kaur, S., Knights, A., Lawton, T., Makepeace, A., Martin, D., Neophytou, M. N., Neville, S., Nieuwenhuijsen, M., Nickless, G., Price, C., Robins, A., Shallcross, D., Simmonds, P., Smalley, R. J., Tate, J., Tomlin, A. S., Wang, H., and Walsh, P. (2004), Introduction to the DAPPLE air pollution project. *Sci. Total Env.*, 332:139–153.

Flaherty, J. E., Lamb, B., Allwine, K. J., and Allwine,

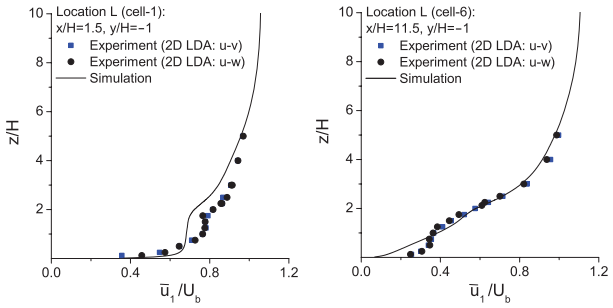

(a) Cell 1 (b) Cell 6

Fig. 11: Comparison of mean velocity at location L in cells 1 and 6 (array-2H).

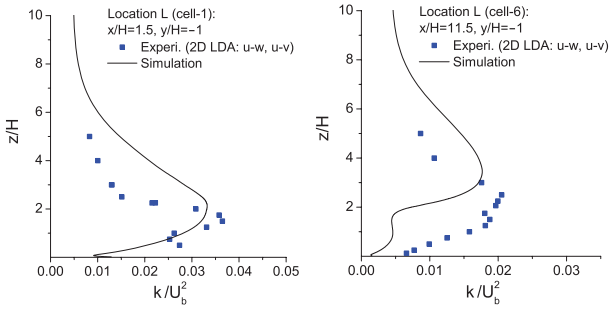

(a) Cell 1 (b) Cell 6

Fig. 12: Comparison of TKE at location L in cells 1 and 6 (array-2H).

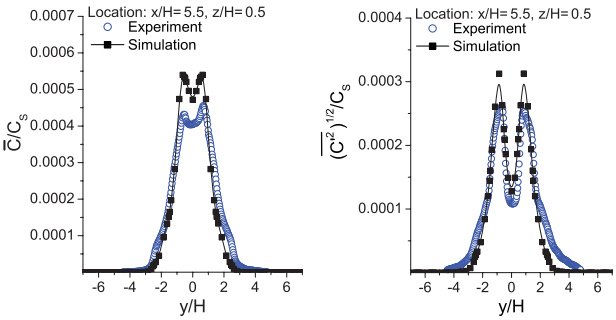

(a) Mean concentration (b) Concentration RMS

Fig. 13: Mean and standard deviation of the concentration at half-canopy height ($z/H = 0.5$) at $x/H = 5.5$ (array-1H).

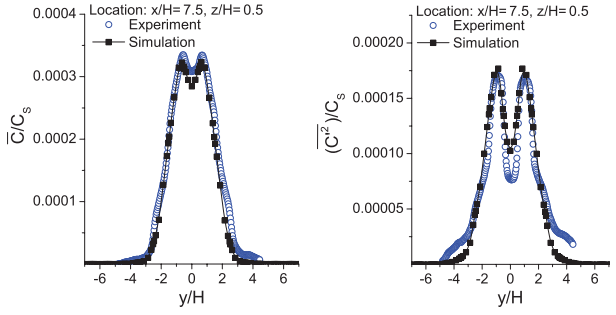

(a) Mean concentration (b) Concentration RMS

Fig. 14: Horizontal profiles of the mean and standard deviation of the concentration at half-canopy height ($z/H = 0.5$) at $x/H = 7.5$ (array-1H).

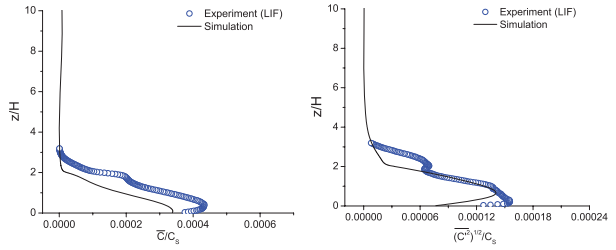

(a) Mean concentration (b) Concentration RMS

Fig. 15: Vertical profiles of the mean and standard deviation of the concentration along the plume centerline ($y/H = 0$) at a downwind distance $x/H = 3.5$ (array-2H).

E. (2007), Vertical tracer concentration profiles measured during the Joint Urban 2003 dispersion study. *J. Appl. Meteorol. Climatol.*, **46**:2019–2037.

Gailis, R. M. and Hill, A. (2006), A wind-tunnel simulation of plume dispersion within a large array of obstacles. *Boundary-Layer Meteorol.*, **119**:289–338.

Hilderman, T. and Chong, R. (2007), A laboratory study of momentum and passive scalar transport and diffusion within and above a model urban canopy. DRDC Suffield CR 2008-025, Defence R&D Canada – Suffield, Ralston, Alberta.

Hsieh, K. J., Lien, F.-S. and Yee, E. (2007), Numerical modeling of scalar dispersion in an urban canopy. *J. Wind Eng. Ind. Aerodyn.*, **95**:1611–1636.

Lien, F.-S. and Leschziner, M. A. (1994), A general non-orthogonal collocated finite volume algorithm for turbulent flow at all speeds incorporating second-moment turbulence-transport closure, Part 1: computational implementation. *Comput. Meth. Appl. Mech. Eng.*, **114**:123–148.

MacDonald, R. W., Griffiths, R. F. and Hall, D. J. (1998), A comparison of results from scaled field and wind tunnel modelling of dispersion in arrays of obstacles. *Atmos. Environ.*, **32**:3845–3862.

Milliez, M. and Carissimo, B. (2008), Computational fluid dynamical modelling of concentration fluctuations in an idealized urban area. *Boundary-Layer Meteorol.*, **127**:241–259.

Pascheke, F., Barlow, J. F. and Robins, A. (2008), Wind-tunnel modelling of dispersion from a scalar area source in urban-like roughness. *Boundary-Layer Meteorol.*, **126**:103–124.

Speziale, C. G. (1987), On nonlinear k-l and k-ϵ models of turbulence. *J. Fluid Mech.* **178**:459-475.

Wang, B.-C., Yee, E. and Lien, F.-S. (2009), Numerical study of dispersing pollutant clouds in a built-up environment. *Int. J. Heat Fluid Flow*, **30**:3–19.

Yee, E. and Biltoft, C. A. (2004), Concentration fluctuation measurements in a plume dispersing through a regular array of obstacles. *Boundary-Layer Meteorol.*, **111**:363–415.

Yee, E., Gailis, R. M., Hill, A., Hilderman, T. and Kiel, D. (2006), Comparison of wind-tunnel and water-channel simulations of plume dispersion through a large array of obstacles with a scaled field experiment. *Boundary-Layer Meteorol.*, **121**:389–432.

Yee, E., Lien, F.-S. and Ji, H. (2007), Technical Description of Urban Microscale Modeling System: Component 1 of CRTI Project 02-0093RD. *DRDC Suffield TR 2007-067*, Defence R&D Canada – Suffield, 55 pages.

Yee, E., Wang, B.-C. and Lien, F.-S. (2009), Probabilistic model for concentration fluctuations in compact-source plumes in an urban environment. *Boundary-Layer Meteorol.*, **130**:169–208.

Yoshizawa, A. (1985), Statistical analysis of the anisotropy of scalar diffusion in turbulent shear flows. *Phys. Fluids*, **28**:3226–3231.